Applied Catalysis B: Environmental 94 (2010) 295–302

Contents lists available at ScienceDirect

Applied Catalysis B: Environmental

journal homepage: www.elsevier.com/locate/apcatb

Effect of calcination temperature on morphology and photoelectrochemical properties of anodized titanium dioxide nanotube arrays

Jiaguo Yu *, Bo Wang

State Key Laboratory of Advanced Technology for Materials Synthesis and Processing, Wuhan University of Technology, Wuhan Luoshi Road 122#, Wuhan 430070, PR China

ARTICLE INFO

Article history:
Received 30 September 2009
Received in revised form 28 November 2009
Accepted 1 December 2009
Available online 4 December 2009

Keywords:
TiO_2 nanotube arrays
Calcination temperature
Photocatalytic activity
Hydroxyl radicals
Photocurrent

ABSTRACT

Highly ordered TiO_2 nanotube arrays (TNs) are prepared by electrochemical anodization of titanium foil in a mixed electrolyte solution of glycerol and NH_4F and then calcined at various temperatures. The prepared samples are characterized by X-ray diffraction, scanning electron microscopy and transmission electron microscopy. The photocatalytic activity is evaluated by photocatalytic degradation of methyl orange (MO) aqueous solution under UV light irradiation. The production of hydroxyl radicals ($^{\bullet}OH$) on the surface of UV-irradiated samples is detected by a photoluminescence (PL) technique using terephthalic acid (TA) as a probe molecule. The transient photocurrent response is measured by several on–off cycles of intermittent irradiation. The results show that low temperatures (below 600 °C) have no great influence on surface morphology and architecture of the TNs sample and the prepared TNs can be stable up to ca. 600 °C. At 800 °C, the nanotube arrays are completely destroyed and only dense rutile crystallites are observed. The photocatalytic activity, formation rate of hydroxyl radicals and photocurrent of the TNs increases with increasing temperatures (from 300 to 600 °C) due to the enhancement of crystallization. Especially, at 600 °C, the sample shows the highest photocatalytic activity due to its bi-phase composition, good crystallization and remaining tubular structures. With further increase in the calcination temperature from 600 to 800 °C, the photocatalytic activity rapidly decreases due to the vanishing of anatase phase, collapse of nanotube structures and decrease of surface areas.

© 2009 Elsevier B.V. All rights reserved.

1. Introduction

Titanium dioxide has been intensively investigated as a semiconductor photocatalytic material for solar energy conversion and environmental purification since Fujishima and Honda discovered the photocatalytic splitting of water on TiO_2 electrodes in 1972 [1]. Among various oxide semiconductor photocatalysts, titania is the most important photocatalyst because of its biological and chemical inertness, nontoxicity, cost effectiveness and strong oxidizing power under UV light irradiation [2–15]. Conventional powder photocatalysts, however, have serious disadvantages and limitations—the need for post-treatment separation from a slurry system after photocatalytic reaction. This can be easily overcome by immobilizing TiO_2 nanoparticles as thin films on a solid substrate. Moreover, these materials would have new industrial applications including antibacterial ceramic tiles, self-cleaning glass and so on [16–18].

It is well known that the photocatalytic activity of TiO_2 thin films strongly depends on the preparing methods and post-treatment conditions, since they have a decisive influence on the physical and chemical properties of TiO_2 thin films. Therefore, it is necessary to investigate the effects of the preparation process and post-treatment conditions on the photocatalytic activity and surface microstructures of the films [19–23]. The TiO_2 thin films are usually prepared by vacuum evaporation, sputtering, chemical vapor deposition (CVD), sol–gel and liquid-phase deposition (LPD) methods [19]. However, these methods have some disadvantages for industry applications. Vacuum evaporation, sputtering, and chemical vapor deposition methods require special apparatuses for deposition of films, the sol–gel method needs coating repeatedly in order to get thick films, and liquid-phase deposition (LPD) requires special raw materials [19–23]. Recently, highly ordered TiO_2 nanotube arrays (TNs) thin films prepared by a simple electrochemical anodization over a titanium substrate have attracted more and more attention since Grimes and his group first prepared the uniform and highly ordered TNs films obtained by anodization of titanium foil in a fluoride containing electrolyte in 2001 [24]. Also, the dimensions of TiO_2 nanotubes can be precisely controlled. Uniform TiO_2 nanotubes of various pore sizes (22–110 nm), lengths (200–1 000 000 nm), and wall thicknesses (7–34 nm) are easily obtained by tailoring electrochemical conditions. A variety of reports in the literature give evidence of the unique properties

* Corresponding author. Tel.: +86 27 87871029; fax: +86 27 87879468.
E-mail address: jiaguoyu@yahoo.com (J. Yu).

0926-3373/$ – see front matter © 2009 Elsevier B.V. All rights reserved.
doi:10.1016/j.apcatb.2009.12.003

this material architecture possesses [25–37], making it of considerable scientific interest as well as practical importance. Considering their large specific surface area, high pore volume, and unique morphology, the obtained NTs will offer new chances to design various 1D TiO_2-related photocatalytic materials by doping, deposition, and sensitization [32,37].

Thermal treatment of TiO_2 and titanate nanotubes provides a facile route to control grain size, particle morphology, microstructures, phase composition and surface photoelectrochemical properties via adjusting experimental parameters such as temperature, time and atmospheres [38–42]. However, few studies have been carried out on the effects of calcination temperature on the morphology and photoelectrochemical properties of the TNs films [26,35]. In this work, we have prepared highly ordered TNs thin films on a titanium foil in a mixed electrolyte solution containing glycerol and NH_4F. The prepared TNs samples were calcined at various temperatures. The effects of calcination temperature on the morphology, structures, crystallization, photocatalytic activity, photoelectrochemical properties of TNs samples were investigated and discussed. To the best of our knowledge, this is the first time to report the effects of calcination temperatures on the photoelectrochemical properties of the TNs. This work may provide new insights for preparing highly photocatalytic activity TiO_2 thin films.

2. Experimental

2.1. Preparation of TiO_2 nanotube arrays

All chemicals used in this study were analytical grade and were used without further purification. Deionized water was used in all experiments. Before electrochemical anodization, Ti foils (0.25 mm, 99% purity) were, respectively, degreased by sonicating in acetone, ethanol and deionized water for each 10 min, and then dried in air. The self-organized TNs were fabricated by anodization of Ti foils in a mixed electrolyte of glycerol and water (50:50 vol.%) + 1 wt.% NH_4F, similarly to the method described by Schmuki and co-worker [36]. Anodization was performed in a two-electrode configuration connected to a DC power supply (RXN-602D, Shenzhen Zhaoxin Electronic Equipment & Instruments Co., China) with titanium foil as the working electrode and platinum foil as the counter electrode under a constant 20 V anodic potential for 2 h at room temperature (25 °C). After anodic oxidation, the as-prepared samples were rinsed with deionized water, and dried in an oven at 80 °C. The resulting amorphous TiO_2 nanotube array samples were calcined at different temperatures (from 300 to 800 °C) for 2 h at a heating rate of 2 °C/min in air to crystallize the tube walls and improve their stoichiometry and crystallization.

2.2. Characterization

The morphology observation was performed on an S-4800 field emission scanning electron microscope (SEM, Hitachi, Japan), which was linked with an Oxford Instruments X-ray analysis system, at an accelerating voltage of 5 kV. Transmission electron microscopy (TEM) and high-resolution transmission electron microscopy (HRTEM) analyses were conducted by a JEM-2100F electron microscope (JEOL, Japan), using a 200 kV accelerating voltage. X-ray diffraction (XRD) patterns obtained on a D/MAX-RB X-ray diffractometer (Rigaku, Japan) using Cu Kα radiation at a scan rate (2θ) of $0.05^\circ\ s^{-1}$ were used to determine the identity of any phase present and their crystallite size. The accelerating voltage and applied current were 40 kV and 80 mA, respectively. The average crystallite size of anatase and rutile grains was quantitatively calculated using Scherrer formula ($d = 0.9\lambda/B\cos\theta$, where d, λ, B and θ are crystallite size, Cu Kα wavelength (0.15418 nm), full width at half maximum intensity (FWHM) of (1 0 1) for anatase and (1 1 0) for rutile peak in radians and Bragg's diffraction angle, respectively) after correcting the instrumental broadening.

2.3. Evaluation of photocatalytic activity

The photocatalytic activity of the TNs samples was characterized by the photocatalytic decolorization of MO aqueous solution at ambient temperature. We chose MO as a probe molecule because MO is a kind of chemically stable and persistent containing-nitrogen dye pollutant [19]. Experimental details were as follows: 2 cm × 2 cm TNs sample was placed in a 5 mL MO aqueous solution with a concentration of 4×10^{-5} M in a 25 mL beaker. The solution was allowed to reach an adsorption–desorption equilibrium among the photocatalyst, MO, and water before UV light irradiation. A 300 W xenon lamp (Changtuo, China) positioned 10 cm away from the beaker was used as a light source to trigger the photocatalytic reaction. One face of the TNs samples was irradiated along the normal direction. The average light intensity striking on the surface of the reaction solution was about 20 mW/cm^{-2}, as measured by a UV meter (made in the photoelectric instrument factory of Beijing Normal University, China) with the peak intensity of 365 nm. The concentration of MO was determined by an UV–visible spectrophotometer (UV-2550, Shimadzu, Japan). After UV light irradiation for some time (every 10 min), the reaction solution was taken out to measure the concentration change of MO. As for the MO aqueous solution with low concentration, its photocatalytic decolorization is a pseudo-first-order reaction and its kinetics may be expressed as $\ln(c_0/c) = kt$, where k is the apparent rate constant, and c_0 and c are the initial and reaction concentrations of aqueous MO, respectively [19].

2.4. Analysis of hydroxyl radicals (•OH)

The formation of hydroxyl radicals (•OH) at the photo-illuminated TNs samples/water interface can be detected by a simple PL method using TA as a probe molecule. TA readily reacts with •OH to produce highly fluorescent product, 2-hydroxyterephthalic acid [37,43]. This method has been used in radiation chemistry, sonochemistry, and biochemistry for the detection of •OH generated in water. The method relies on the PL signal at 425 nm of 2-hydroxyterephthalic acid. The PL intensity of 2-hydroxyterephthalic acid is proportional to the amount of •OH radicals produced in water. The method is simple, rapid, sensitive, and specific and needs only a simple standard PL instrumentation. Experimental procedures are similar to the measurement of photocatalytic activity except that MO aqueous solution was replaced by the 5×10^{-4} M TA aqueous solution with a concentration of 2×10^{-3} M NaOH solution. PL spectra of generated 2-hydroxyterephthalic acid were measured on a Hitachi F-7000 fluorescence spectrophotometer (Hitachi, Japan). After light irradiation for every 10 min, the reaction solution was used to measure the increase of the PL intensity at 425 nm excited by 315 nm light [37].

2.5. Photoelectrochemical measurements

Photoelectrochemical characterization was carried out with a set-up consisting of a 300 W xenon lamp as an UV light source, and the light intensity was about 20 mW/cm^2. Photocurrents were measured using an electrochemical analyzer (CHI660C Instruments, CHI, China) in a standard three-electrode system with the prepared samples as the working electrodes with an active area of ca. 0.5 cm^2, a Pt wire as the counter electrode, and Ag/AgCl

(saturates KCl) as a reference electrode. A 1 M Na_2SO_4 aqueous solution was used as the electrolyte [37].

3. Results and discussion

3.1. SEM and XRD studies

The self-organized TiO_2 nanotube arrays were synthesized by anodic oxidation of Ti foils and then annealed in air at 300, 400, 500, 600, 700 and 800 °C for 2 h to obtain the crystallization samples (see Section 2). The morphologies of the TNs samples were observed using SEM. Fig. 1a shows a typical SEM image of the uncalcined TNs. Uniform and highly ordered nanotube arrays grown on a Ti substrate are observed. The as-prepared samples before calcination are found to have an average pore diameter of ca. 80 nm and wall thickness of ca. 30 nm. The inset in Fig. 1a is a cross-sectional view of the TNs, indicating that the TNs are composed of well-aligned nanotubes of about 1.9 μm in length which grow vertically from a Ti substrate. The composition of the TNs was determined by energy dispersive X-ray spectroscopy (EDX) experiments. EDX analysis (not shown here) demonstrates that the as-prepared samples contain Ti, O and a small amount of F element, confirming TNs consisting of TiO_2. F element is from the precursor NH_4F due to surface adsorption [8]. However, no signal of F is observed in the other calcined samples when calcination temperature is higher than 400 °C, revealing the F impurity could

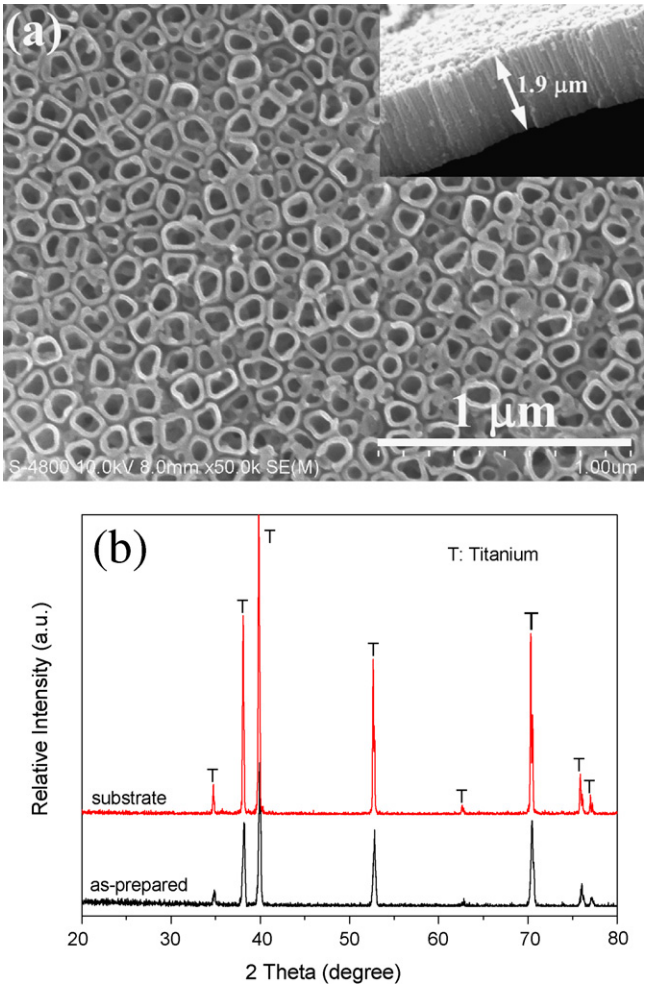

Fig. 1. (a) A typical top view SEM image of the as-prepared TNs, the inset in (a) showing the cross-sectional SEM image of as-prepared TNs; (b) XRD patterns of the as-prepared TNs and Ti substrate.

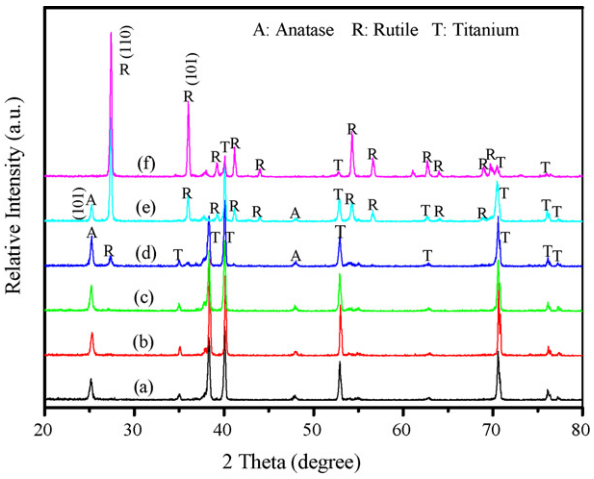

Fig. 2. XRD patterns of TNs samples calcined at 300 °C (a), 400 °C (b), 500 °C (c), 600 °C (d), 700 °C (e) and 800 °C (f) in air for 2 h.

be easily removed by calcination. Fig. 1b shows the comparison of XRD patterns of as-prepared TNs and Ti substrate. For Ti substrate, all the diffraction peaks corresponding to titanium metal phase (JCPDS 44-1294) indicate only pure titanium existing in the Ti substrate. On the other hand, for the as-prepared TNs, the peaks corresponding to titanium metal phase still can be observed and no peak of any TiO_2 phases (anatase, rutile or brookite) exists, which indicates that the as-prepared TNs are an amorphous phase before calcination.

It is well known that understanding the mechanism of the phase transformation of a material is fundamental to the control of the microstructure and, thus, the material properties [44]. The phase structure and composition, crystallite size and crystallinity of TiO_2 are of great influence on its photocatalytic activity and photoelectrochemical properties [7,19,20]. Therefore, XRD was used to analyze the changes of phase structures and crystallite sizes of the calcined TNs samples. Fig. 2 shows XRD patterns of the TNs samples calcined at various temperatures. It can be seen that the calcination temperatures obviously influence on the crystallization and phase structures of the TNs samples. For 300 °C-calcined samples, except the diffraction peaks of Ti substrate, two broad peaks at $2\theta = 25.3°$ and 48.1°, respectively, corresponding to (1 0 1) and (2 0 0) plane diffraction of anatase TiO_2 (JPCDS 21-1272) are clearly observed (Fig. 2a). With increasing calcination temperatures (from 300 to 600 °C), XRD peak intensities of anatase steadily become stronger and the width of XRD diffraction peaks of anatase becomes narrower, indicating the formation of greater TiO_2 crystallites and enhancement of crystallization. The crystallinity of TiO_2 was quantitatively evaluated via the relative intensity of the (1 0 1) diffraction peak of the anatase. Table 1 lists the average crystalline sizes and relative anatase crystallinity of TNs samples calcined at different temperatures. It can be seen that the average crystalline sizes and relative anatase crystallinity increase with increasing calcination temperatures. However, at 600 °C, a small peak at $2\theta = 27.5°$ corresponding to (1 1 0) plane diffraction of rutile (JPCDS 87-920) appears, suggesting the occurrence of phase transformation of anatase to rutile. Surprisingly, at this temperature, the average crystallite size of anatase decreases slightly (from 30.5 to 29.9 nm) and 28.1% of the anatase TiO_2 is transformed into rutile TiO_2 (Table 1). Our previous investigations indicate that the phase transformation causes the growth of crystallite size of anatase due to the heat of phase transformation in situ to accelerate grain growth [7,19,20]. Why does the anatase-to-rutile phase transformation cause the decrease of the average crystallite in this study? One possible explanation is that greater

Table 1
Effects of calcination temperatures on phase structures and average crystallite size of TNs.

Temperature (°C)	Un-calcined	300	400	500	600	700	800
Phase content (%)[a]	Am	A	A	A	71.9(A) 28.1(R)	12.0(A) 88.0(R)	R
Relative crystallinity[b]	–	1	1.06	1.19	1.39(A)	–	–
Crystalline size (nm)	–	25.2	25.5	30.5	29.9(A) 34.5(R)	29.3(A) 37.8(R)	>180

[a] Am, A and R denote amorphous, anatase and rutile, respectively.
[b] Relative anatase crystallinity: the relative intensity of the diffraction peak from the anatase (1 0 1) plane (reference = the 300 °C-calcined sample).

anatase crystallites first turn into rutile during the phase transformation, which results in the decrease of average crystallite size of anatase. It should be noted that Grimes et al. also reported the similar results [26]. At 700 °C, the intensity of rutile diffraction peak increases sharply, indicating that most anatase phase is transformed into rutile phase. At this temperature, the mass fraction of rutile is 88%, and its crystallite size is 37.8 nm. At 800 °C, anatase completely turns into rutile phase and the crystallite size of rutile markedly increases to more than 180 nm (see Table 1 and Fig. 3d). Further observation indicates that the diffraction peaks from the titanium substrates obviously decrease with increasing temperature. Especially, at 800 °C, the diffraction peaks of titanium almost vanish. The similar phenomenon are also reported by Grimes et al. and they suggest that titanium is directly oxidized and transformed into rutile titania at high temperatures [26]. Why does the crystallite size of rutile rapidly increase from about 30 to more than 180 nm? This is due to the phase transformation heat of anatase to rutile and titanium to rutile in situ to accelerate the growth of rutile crystallites [7,19,20].

Fig. 3 shows effects of calcination temperatures on the morphology of TNs. It can be observed from Fig. 3a that the 600 °C-calcined TNs samples still keep their original morphology, confirming that the prepared TNs has high mechanical strength and thermal stability. From 300 to 500 °C, the TNs samples have a similar surface morphology to the 80 °C-dried and 600 °C-calcined samples and the pore diameter and wall thickness of the nanotubes have no obvious change (not shown here). This indicates that low temperatures (below 600 °C) have no great influence on surface morphology and architecture of the TNs sample and the prepared TNs can be stable up to ca. 600 °C. It should be noted that at 600 °C, the crystallite size (34.5 nm) of rutile phase is larger than the thickness (ca. 30 nm) of tube walls, however, which have no obvious change observed. This implies that the nucleation of rutile phase preferentially take place at the interface between the substrates and TNs [26,44], which makes the TNs maintaining stable tubular structures above the substrate. This leads to an excellent thermal stability of TNs till around 600 °C even after the crystallization of rutile phase occurs at the interface of TNs and Ti substrate. TEM image (see Fig. 3e) clearly indicates that the 600 °C-calcined sample has stable tubular structures. At 700 °C, the surface morphology of calcined TNs has a great change (Fig. 3b). The tubular structures are difficult to observe due to destruction and coalescence at the top of nanotube walls. The surface of calcined nanotubes becomes aggregates of TiO_2 particles with diameters of 35–40 nm. Fig. 3c presents a region SEM image of the 700 °C-calcined TNs sample. It is revealed that tubular channels still kept in the middle of the TNs, which is ascribed to remaining anatase phase. When the calcination temperature increases to 800 °C, the nanotube arrays are completely destroyed and only dense rutile crystallites with size of over 180 nm are observed (Fig. 3d), which is attributed to the fact that high temperature and phase-transformation heat cause the sintering and growth of rutile crystallites, on the other hand, the diffusion of oxygen in air into the nanotube–support interface region oxidize the titanium in that region and directly transform titanium into rutile phase [26]. These rutile grains continue to grow with temperature and they consume the nanotubes to produce a dense rutile film (Fig. 3d). Fig. 3f shows TEM image of the 800 °C-calcined samples and corresponding HRTEM image (inset in Fig. 3f) taken at the edge of a nanoparticle (marking in a cycle in Fig. 3f) and electron diffraction pattern (inset in Fig. 3f), indicating that the rutile crystallite rapidly increase from about 30 to more than 180 nm. HRTEM image and electron diffraction pattern further confirm that single nanoparticle is single crystal. The above results suggest that the phase transformation of anatase to rutile first occurs at the interface between Ti substrates and TNs, then on the top of nanotubes, finally on the bulk of nanotubes. The first interface phase transformation from anatase to rutile has no obvious influence on the morphology, contrarily, the second surface phase transformation, especially third bulk phase transformation, results in the significant changes of surface architecture and crystallite size of TiO_2 (Fig. 3d).

On the basis of the above results and discussion, we suggest a model to explain the anatase-to-rutile phase transformation and morphology architecture evolution of TNs samples, which is schematically represented in Fig. 4. The nucleation and growth of rutile phase first occur at the interface between TiO_2 nanotubes and Ti substrate at 600 °C. These crystallites grow in size with increasing temperature. At 700 °C, the surface nucleation and growth of rutile phase are observed on the surface of TiO_2 nanotube arrays. At 800 °C, the bulk nucleation and growth of rutile phase are observed within TiO_2 nanotube arrays, resulting in the rapid growth of rutile grains, destroy of tubular architectures and formation of coarsened rutile film. According to the viewpoint of Zhang and Banfield, the interface nucleation (IN) of rutile has the lowest activation energy of nucleation [44]. Therefore, it is not surprising that the anatase-to-rutile phase transformation first occur at the nanotube–substrate interface. Furthermore, Zhang and Banfield point out that for Ti and O atoms on the surface of an anatase particle, their coordination numbers are less than those of atoms in the bulk; thus, more chemical bonds have to be broken in bulk nucleation (BN). Accordingly, it is expected that the activation energy for bulk nucleation is greater than that for surface nucleation (SN) and a stronger thermal fluctuation is needed, and thus, very high temperatures are required [44]. Therefore, it is not difficult to understand that the relative magnitude of the activation energies for interface nucleation, surface nucleation, and bulk nucleation can be expressed in the order $E_a(\mathrm{IN}) < E_a(\mathrm{SN}) < E_a(\mathrm{BN})$. The difference of E_a leads to a strong temperature dependence of the nucleation mechanism of rutile phase [44]. Consequently, we can use their theory to reasonably explain our experimental observation, interface nucleation predominates at a relative low temperature (600 °C), surface nucleation predominates at intermediate temperatures (700 °C), and bulk nucleation predominates at very high temperatures (800 °C).

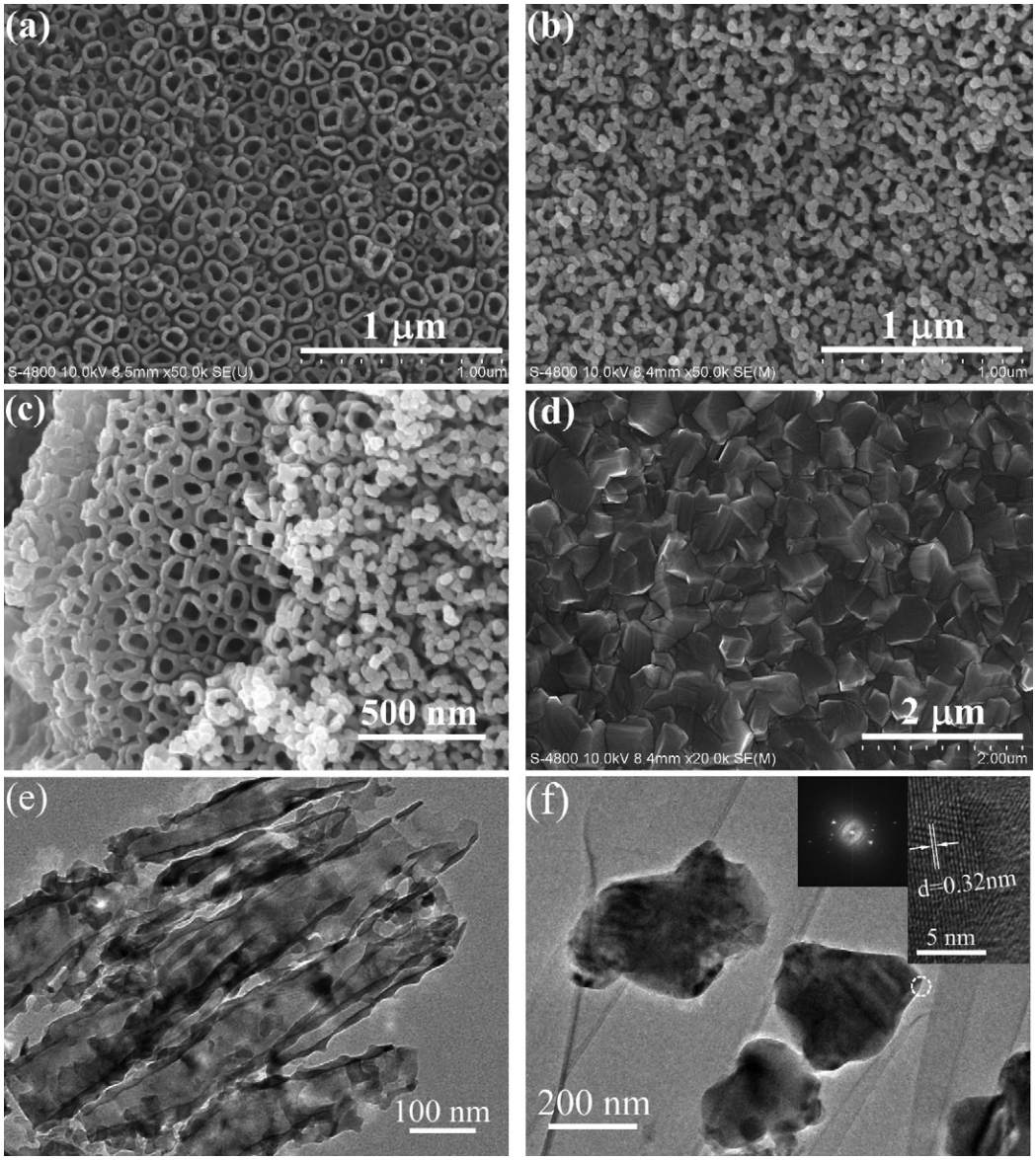

Fig. 3. SEM images of the TNs samples calcined at 600 °C (a), 700 °C (b and c) and 800 °C (d) and TEM images of the samples calcined at 600 °C (e) and 800 °C (f). Inset in (f) showing corresponding HRTEM image and electron diffraction pattern of the 800 °C-calcined sample.

3.2. Photocatalytic activity

The photocatalytic activity of the samples was evaluated by photocatalytic degradation decolorization of MO aqueous solution under UV light irradiation. However, under dark conditions without light illumination, the MO concentration does not change for every measurement using various TNs samples. Illumination in the absence of TNs does not result in the photocatalytic decolorization of MO. Therefore, the presence of both illumination and TNs is necessary for the efficient degradation. These results also suggest that the degradation decolorization of MO aqueous solution is caused by photocatalytic reactions on TNs surface under the UV illumination.

Fig. 5 shows the comparison of photocatalytic activity of the samples before and after calcination at different temperatures. It can be seen that the calcination temperatures have a great

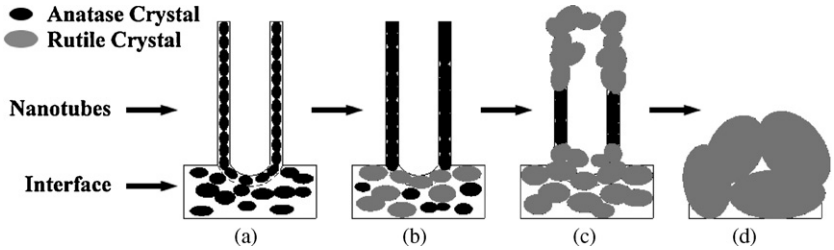

Fig. 4. Schematic diagram of the anatase-to-rutile phase transformation and morphology evolution of the TNs samples calcined at 500 °C (a), 600 °C (b), 700 °C (c) and 800 °C (d).

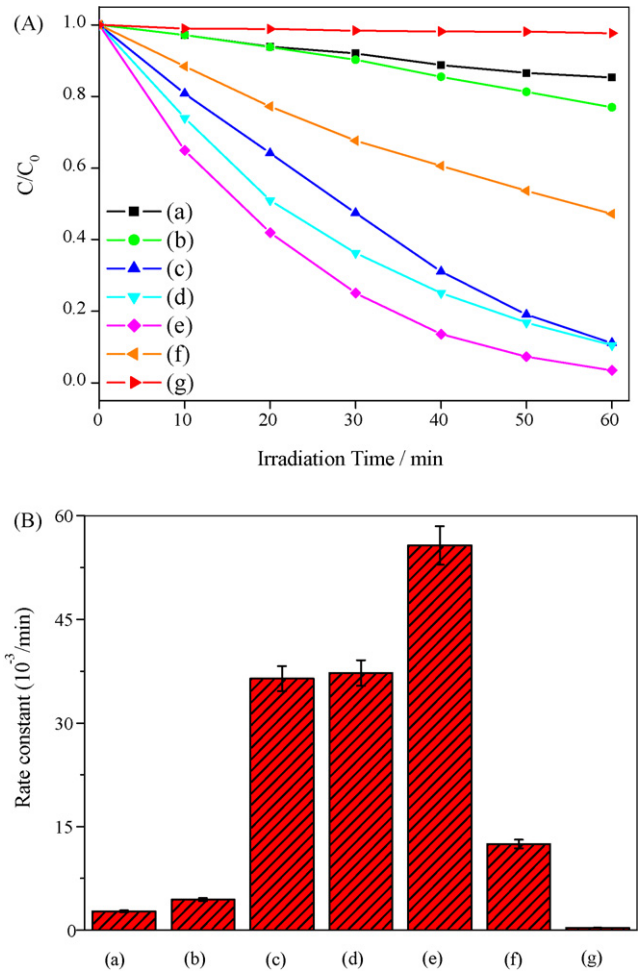

Fig. 5. Comparison of photocatalytic activity of the samples calcined at various temperatures for the photocatalytic decomposition of MO in water: (a) as-prepared TNs, (b) 300 °C, (c) 400 °C, (d) 500 °C, (e) 600 °C, (f) 700 °C and (g) 800 °C. (A) C/C_0–t curve, C and C_0 denote the reaction and initial concentration of MO in the system, respectively. (B) The apparent rate constants.

influence on the photocatalytic activity of the TNs. Although the as-prepared TNs sample has tubular structures and large porous surface area, a weak photocatalytic activity is observed due to its amorphous phase structure. At 300 °C, the calcined sample also shows a relative low photocatalytic activity. This is due to the weak crystallization of TiO_2 in the sample [20,45]. With increasing the calcination temperature to 400 and 500 °C, the photocatalytic activity obviously increases owing to the enhancement of TiO_2 crystallization and the decrease of defects in the samples (see Fig. 3 and Table 1). At 600 °C, the sample shows the highest photocatalytic activity and its k reaches 0.056 min^{-1}. The k was determined to be 0.0044 min^{-1} for the 300 °C-calcined sample. The photocatalytic activity of the 600 °C-calcined sample exceeds that of the 300 °C-calcined sample by a factor of 12.7, which is attributed to the following fact that, first, the 600 °C-calcined sample exhibits the best crystallization (see Table 1), usually, the crystallization is an important factor influencing the photocatalytic activity [7–9]. Second, the sample contains anatase (ca. 72% in mass percentage) and rutile (ca. 28%) two phases (Table 1), it is well known that the composite of two kinds of semiconductors or two phases of the same semiconductor is beneficial in reducing the combination of photo-generated electrons and holes and enhancing photocatalytic activity [46–48]. Finally, the 600 °C-calcined sample still maintains ordered tubular structures with no obvious change in pore diameter or wall thickness, resulting in large pore surface areas. For TiO_2 catalysts, large surface areas can provide more active sites and photocatalytic reaction centers for the adsorption of reactant molecules [48]. Moreover, highly ordered tubular structures can provide a straight diffusion path for reactant molecules from the solution to the active surface area and enhance the adsorption efficiency of light [30]. Therefore, it is not surprising that the 600 °C-calcined sample has the best photocatalytic activity. With further increasing the calcination temperature to 700 °C, the photocatalytic activity decreases. This is ascribed to the following two causes. The first cause is due to most of the anatase phase changing into rutile phase (88%), which has the lowest photocatalytic activity among three different crystalline phases of TiO_2 (anatase, brookite and rutile) [47]. Our previous investigation has indicated that the composition of two phases also obviously influences photocatalytic activity and an optimal brookite to anatase mass ratio (3:7) is observed [48]. Furthermore, it is well known that Degussa P25 (P25) has superior photocatalytic activity due to P25 containing anatase (78% in mass fraction) and rutile (22%) two-phase structures. The above results and discussion imply that the mass ratios of rutile to anatase also obviously influence photocatalytic activity, and an optimal rutile to anatase mass ratio also is ca. 3:7. The second cause is due to destroy of architectures and tubular structures of TNs, resulting in the rapid decrease of photocatalytic activity. At 800 °C, there is no photocatalytic activity observed. This is attributed to the formation of full rutile phase, the sintering and growth of dense rutile crystallites and the disappearance of porous surface areas. Usually, rutile shows neglectable photocatalytic activity or no photocatalytic activity [46,47].

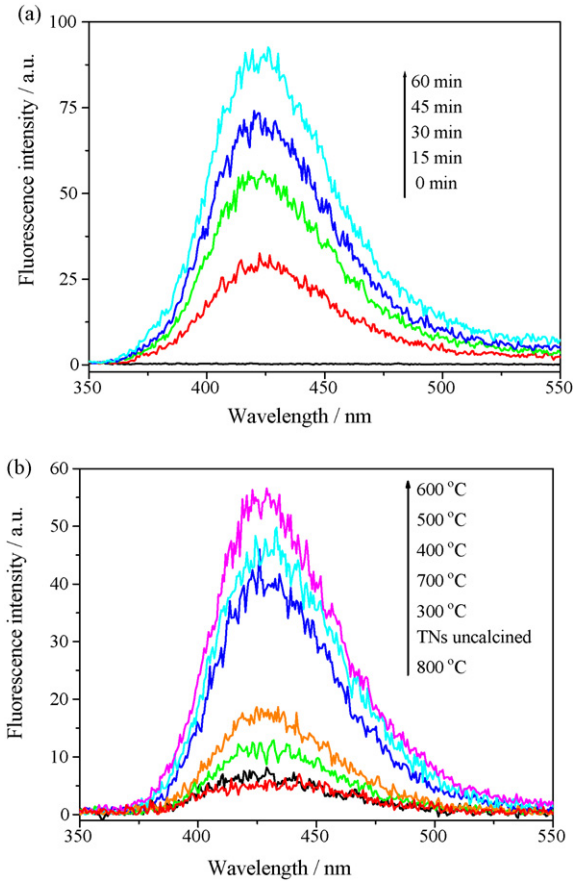

Fig. 6. (a) PL spectral changes with UV light irradiation time on the 600 °C-calcined sample in a 5×10^{-4} M basic solution of TA (excitation at 315 nm) and (b) PL spectra of the samples calcined at various temperatures in a 5×10^{-4} M basic solution of TA under UV light irradiation at a fixed 30 min.

3.3. Hydroxyl radical analysis

The photocatalytic activity of the prepared samples was further confirmed by the detection of •OH. Fig. 6a shows the changes of PL spectra of TA solution under UV light irradiation with irradiation time. A gradual increase in PL intensity at about 425 nm is observed with time for the 600 °C-calcined sample. However, no PL increase is observed in the absence of UV light irradiation or TNs samples. This suggests that the fluorescence is from the chemical reactions between TA and •OH produced during photocatalytic reactions [37,43]. Fig. 6b shows the comparison of PL intensity for different calcined samples illumined for 30 min. Usually, PL intensity is proportional to the amount of produced hydroxyl radicals [37,43]. At a fixed time (30 min), the amount of OH radicals produced on the 600 °C-calcined sample is larger than that of OH radicals produced on all other samples. This also suggests that the 600 °C-calcined sample has the highest photocatalytic activity. Further observation shows that weak PL signals or no PL signals are observed for the 80 °C-dried and 800 °C-calcined sample, implying weak photocatalytic activity or no photocatalytic activity for these samples. Our hydroxyl radical experiments further confirm that hydroxyl radicals are active species during photocatalytic reactions. On the other hand, the formation rate of OH radicals has a positive relation with the photocatalytic activity.

3.4. Transient photocurrent response

To further investigate and understand photocatalytic mechanism, the transient photocurrent responses of the TNs samples calcined at different temperatures are measured by several on–off cycles of intermittent irradiation. Fig. 7 shows a comparison of *I*–*t* curves of different samples. It can be seen that the photocurrent value rapidly decreases to zero as soon as the irradiation of light turns off, and the photocurrent comes back to a constant value when the light is again on, which has a good reproducibility. This indicates that under UV light irradiation, most of the photo-generated electrons are transported to the walls of TiO_2 nanotubes, and then transferred to titanium substrate to produce photocurrent. The photocurrent curves of different samples all have an anodic photocurrent spike at the initial time of irradiation. This initial current is due to the separation of electron–hole pairs at the TiO_2/electrolyte interface: holes are trapped or captured by reduced species in the electrolyte, while the electrons are transported to the back contact substrate via the walls of TiO_2 nanotubes. After the spike current has been attained, a continuous decrease of the photocurrent with time can be observed until a constant current is reached [48,49]. The photocurrent decay indicates that recombination processes are occurring. Holes reaching the TiO_2 nanotube surface may, instead of capturing electrons from the electrolyte, accumulate at the surface and recombine with electrons from TiO_2 conduction band; that is, the decay is determined by the rate at which minority carriers trapped at surface states capture majority carriers. Another recombination process giving rise to a decay of the photocurrent is that conduction band electrons start to reduce photo-generated oxidized species in the electrolyte [48,49]. After recombination of the excessive holes with electrons, the generation and transfer of electron–hole pairs reach an equilibration, observing a constant current. Further observation indicates that calcination temperature also has great effects on the size of the photocurrent. The TNs samples calcined below 600 °C have less photocurrent due to their weak crystallization resulting in more defects in the tube walls. At 600 °C, the sample shows the biggest photocurrent due to its bi-phase structure, good crystallization and remaining tubular structures. With further increasing calcination temperature to 700 °C, the photocurrent rapidly decreases due to the decrease of anatase content, destroy of the tubular channels and increase of electron–hole recombination rates. At 800 °C, there is a very low photocurrent observed owing to the formation of dense rutile film. The photocatalytic activity of TiO_2 usually depends on a competition between the following two processes, that is, the ratio of the transfer rate of surface charge carriers from the interior to the surface to the recombination rate of photo-generated electrons and holes. If the recombination of photo-generated electrons and holes occurs too fast (<0.1 ns), then there is not enough time for any other chemical reaction to occur. Compared with other semiconductor, the surface charge carriers of TiO_2 are relatively long-lived (around 250 ns), allowing the electrons or holes to travel to the crystallite surface [50,51]. This implies that rutile TiO_2 has a greater recombination rate of photo-generated electrons and holes than anatase and charge carriers cannot transfer to the surface from the interior. Therefore, it is not surprising that rutile exhibits neglectable photocurrent and photocatalytic activity [50–54].

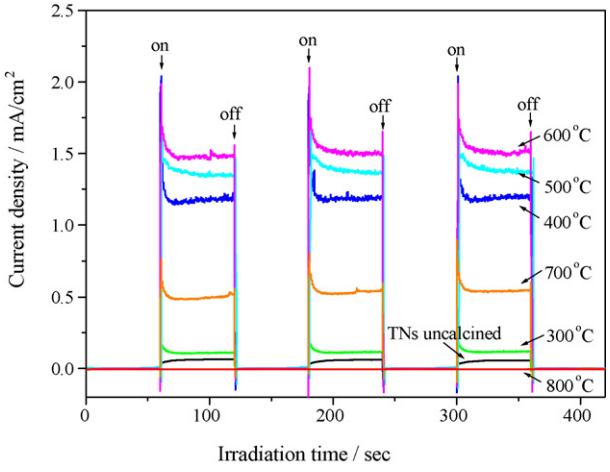

Fig. 7. Comparison of transient photocurrent response of TNs samples calcined at different temperatures in 1 M Na_2SO_4 aqueous solutions under UV light irradiation at +0.0 V vs. Ag/AgCl.

4. Conclusions

Highly ordered TiO_2 nanotube arrays can be easily prepared by electrochemical anodization of titanium foil. Calcination temperatures exhibit a great influence on the architectures and photoelectrochemical properties of the TiO_2 nanotube arrays. Low temperatures (below 600 °C) have no great influence on surface morphology and architecture of the TNs sample and the prepared TNs can be stable up to ca. 600 °C. When the calcination temperature increases to 800 °C, the nanotube arrays are completely destroyed and only dense rutile crystallites are observed. With increasing calcination temperatures from 300 to 600 °C, photocatalytic activity, formation rate of hydroxyl radicals and photocurrent of the samples markedly increase due to the formation of anatase and enhancement of crystallization. At 600 °C, the sample shows the highest photocatalytic activity and biggest formation rate of hydroxyl radicals and photocurrent because of its bi-phase structures, good crystallization and remaining tubular structures. At 700 to 800 °C, the photocatalytic activity of the samples rapidly decreases due to the formation of rutile phase, collapse of tubular structures and decrease of porous surface area.

Acknowledgements

This work was partially supported by the National Natural Science Foundation of China (50625208, 20773097 and

20877061). This work was also financially supported by the National Basic Research Program of China (2007CB613302 and 2009CB939704) and CHCL09006.

References

[1] A. Fujishima, K. Honda, Nature 238 (1972) 637.
[2] L.G. Devi, N. Kottam, S.G. Kumar, J. Phys. Chem. C 113 (2009) 15593.
[3] M.R. Hoffmann, S.T. Martin, W. Choi, D.W. Bahnemann, Chem. Rev. 95 (1995) 69.
[4] M. Ksibi, S. Rossignol, J.M. Tatibouet, C. Trapalis, Mater. Lett. 62 (2008) 4204.
[5] H. Kim, W. Choi, Appl. Catal. B 69 (2007) 127.
[6] L.G. Devi, B.N. Murthy, S.G. Kumar, Chemosphere 76 (2009) 1163.
[7] J.C. Yu, J.G. Yu, W.K. Ho, Z.T. Jiang, L.Z. Zhang, Chem. Mater. 14 (2002) 3808.
[8] J.G. Yu, W.G. Wang, B. Cheng, B.L. Su, J. Phys. Chem. C 113 (2009) 6743.
[9] J.G. Yu, Q.J. Xiang, M.H. Zhou, Appl. Catal. B 90 (2009) 595.
[10] S.W. Liu, J.G. Yu, S. Mann, J. Phys. Chem. C 113 (2009) 10712.
[11] F.B. Li, X.Z. Li, Appl. Catal. A 228 (2002) 15.
[12] H. Lachheb, E. Puzenat, A. Houas, M. Ksibi, E. Elaloui, C. Guillard, J.M. Herrmann, Appl. Catal. B 39 (2002) 75.
[13] M. Vautier, C. Guillard, J.M. Herrmann, J. Catal. 201 (2001) 46.
[14] J. Fernandez, J. Kiwi, J. Baeza, J. Freer, C. Lizama, H.D. Mansilla, Appl. Catal. B 48 (2004) 205.
[15] Y.X. Li, G.X. Lu, S.B. Li, J. Photochem. Photobiol. A 152 (2002) 219.
[16] J.C. Yu, J.G. Yu, J.C. Zhao, Appl. Catal. B 36 (2002) 31.
[17] J.G. Yu, X.J. Zhao, Q.N. Zhao, Mater. Chem. Phys. 69 (2001) 25.
[18] C. Trapalis, A. Gartner, M. Modreanu, G. Kordas, A. Anastasescu, R. Scurtu, M. Zaharescu, Appl. Surf. Sci. 253 (2006) 367.
[19] J.G. Yu, H.G. Yu, B. Cheng, X.J. Zhao, J.C. Yu, W.K. Ho, J. Phys. Chem. B 107 (2003) 13871.
[20] J.G. Yu, J.F. Xiong, B. Cheng, S.W. Liu, Appl. Catal. B 60 (2005) 211.
[21] M.H. Zhou, J.G. Yu, S.W. Liu, P.C. Zhai, L. Jiang, J. Hazard. Mater. 154 (2008) 1141.
[22] K. Kato, A. Tsuzuki, Y. Torii, H. Taoda, T. Kato, Y. Butsugan, J. Mater. Sci. 30 (1995) 837.
[23] M.F.J. Dijkstra, A. Michorius, H. Buwalda, H.J. Panneman, J.G.M. Winkelman, A.A.C.M. Beenackers, Catal. Today 66 (2001) 487.
[24] D. Gong, C.A. Grimes, O.K. Varghese, W.C. Hu, R.S. Singh, Z. Chen, E.C. Dickey, J. Mater. Res. 16 (2001) 3331.
[25] K. Shankar, G.K. Mor, A. Fitzgerald, C.A. Grimes, J. Phys. Chem. C 111 (2007) 21.
[26] O.K. Varghese, D.W. Gong, M. Paulose, C.A. Grimes, E.C. Dickey, J. Mater. Res. 18 (2003) 156.
[27] J.M. Macak, H. Tsuchiya, P. Schmuki, Angew. Chem. Int. Ed. 44 (2005) 2100.
[28] G.K. Mor, O.K. Varghese, M. Paulose, K. Shankar, C.A. Grimes, Sol. Energy Mater. Sol. Cells 90 (2006) 2011.
[29] J.H. Park, S. Kim, A.J. Bard, Nano Lett. 6 (2006) 24.
[30] J.M. Macak, M. Zlamal, J. Krysa, P. Schmuki, Small 3 (2007) 300.
[31] S.P. Albu, A. Ghicov, J.M. Macak, R. Hahn, P. Schmuki, Nano Lett. 7 (2007) 1286.
[32] W.T. Sun, Y. Yu, H.Y. Pan, X.F. Gao, Q. Chen, L.M. Peng, J. Am. Chem. Soc. 130 (2008) 1124.
[33] H.C. Liang, X.Z. Li, Appl. Catal. B 86 (2009) 8.
[34] Y.S. Sohn, Y.R. Smith, M. Misra, V. Subramanian, Appl. Catal. B 84 (2008) 372.
[35] S.P. Albu, A. Ghicov, S. Aldabergenova, P. Drechsel, D. LeClere, G.E. Thompson, J.M. Macak, P. Schmuki, Adv. Mater. 20 (2008) 4135.
[36] J.M. Macak, P. Schmuki, Electrochim. Acta 52 (2006) 1258.
[37] J.G. Yu, G.P. Dai, B.B. Huang, J. Phys. Chem. C 113 (2009) 16394.
[38] G. Li, Z.Q. Liu, J. Lu, L. Wang, Z. Zhang, Appl. Surf. Sci. 255 (2009) 7323.
[39] J.G. Yu, H.G. Yu, B. Cheng, C. Trapalis, J. Mol. Catal. A 249 (2006) 135.
[40] P. Charoensirithavorn, Y. Ogomi, T. Sagawa, S. Hayase, S. Yoshikawaa, J. Electrochem. Soc. 156 (2009) H803.
[41] M. Qamar, C.R. Yoon, H.J. Oh, D.H. Kim, J.H. Jho, K.S. Lee, W.J. Lee, H.G. Lee, S.J. Kim, Nanotechnology 17 (2006) 5922.
[42] L. Zhao, J.G. Yu, J.J. Fan, P.C. Zhai, S.M. Wang, Electrochem. Commun. 11 (2009) 2052.
[43] K. Ishibashi, A. Fujishima, T. Watanabe, K. Hashimoto, Electrochem. Commun. 2 (2000) 207.
[44] H.Z. Zhang, J.F. Banfield, J. Mater. Res. 15 (2000) 437.
[45] J.G. Yu, H.G. Yu, C.H. Ao, S.C. Lee, J.C. Yu, W.K. Ho, Thin Solid Films 496 (2006) 273.
[46] J.G. Yu, Y.R. Su, B. Cheng, Adv. Funct. Mater. 17 (2007) 1984.
[47] J.G. Yu, L.J. Zhang, B. Cheng, Y.R. Su, J. Phys. Chem. C 111 (2007) 10582.
[48] J.G. Yu, S.W. Liu, H.G. Yu, J. Catal. 249 (2007) 59.
[49] A. Hagfeldt, H. Lindström, S. Södergren, S.E. Lindquist, J. Electroanal. Chem. 381 (1995) 39.
[50] J. Ovenstone, J. Mater. Sci. 36 (2001) 1325.
[51] M.H. Zhou, J.G. Yu, B. Cheng, J. Hazard. Mater. 137 (2006) 1838.
[52] W. Choi, A. Termin, M.R. Hoffmann, J. Phys. Chem. 98 (1994) 13669.
[53] H. Einaga, T. Ibusuki, S. Futamura, Environ. Sci. Technol. 38 (2004) 285.
[54] S. Ardizzone, C.L. Bianchi, G. Cappelletti, S. Gialanella, C. Pirola, V. Ragaini, J. Phys. Chem. C 111 (2007) 13222.